Journal of Sound and Vibration (2002) **249**(4), 719–741
doi:10.1006/jsvi.2001.3880, available online at http://www.idealibrary.com on IDEAL®

MERGING SENSOR DATA FROM MULTIPLE MEASUREMENT SET-UPS FOR NON-STATIONARY SUBSPACE-BASED MODAL ANALYSIS

L. MEVEL[†]

IRISA, Campus de Beaulieu, 35042 *Rennes Cedex, France*

M. BASSEVILLE[‡]

IRISA, Campus de Beaulieu, 35042 *Rennes Cedex, France. E-mail: basseville@irisa.fr*

A. BENVENISTE[†]

IRISA, Campus de Beaulieu, 35042 *Rennes Cedex, France*

AND

M. GOURSAT

INRIA, BP 105, *Rocquencourt*, 78153 *Le Chesnay Cedex, France*

(*Received* 19 *February* 2001, *and in final form* 29 *June* 2001)

Processing sensor data, from multiple non-simultaneously recorded measurement set-ups, for structural analysis is often achieved by merging identification results obtained from records corresponding to different sensor pools. Since pole matching and eigenvector gluing might not be consistent in some cases, the question arises to merge the data first and then process them globally. Subspace identification algorithms have proven efficient for performing output-only modal analysis of mechanical systems subject to uncontrolled, unmeasured, and non-stationary excitation. The purpose of this paper is to investigate as to how subspace-based output-only modal analysis algorithms can be adapted to handle the multi-patch measurements set-up. Numerical results, obtained on both laboratory and real application examples, are reported, which show the relevance and usefulness of the proposed algorithm.

1. INTRODUCTION

A major issue for in-operation structural vibration analysis, based on measurements from accelerometers or strain gauges, is to identify modes and modal shapes of mechanical systems subject to an uncontrolled, *unmeasured* and *non-stationary* excitation [1, 2]. Typical examples are offshore structures subject to swell, buildings subject to wind or earthquake, bridges subject to traffic, dams, wings subject to flutter in flight, and turbines subject to steam turbulence, friction in bearings, and imperfect balancing. Modelling modes and modal shapes through state-space representations [3–5] shows that structural analysis is an important instance of identification of the eigenstructure of a linear multi-variable system

[†]Also with INRIA
[‡]Also with CNRS

0022-460X/02/040719 + 23 $35.00/0

[6–9]. For linear system identification, subspace-based methods [10–12] have proven efficient.

In-operation structural analysis calls for the use of *output-only* identification methods [13, 14]. The non-stationarity of the unknown excitation also calls for processing long samples of multi-sensor output measurements, and for using *covariance-driven* subspace-based identification methods [15, 16].

A classical approach in structural analysis consists in processing data measured with respect to multiple references. This approach is called polyreference modal analysis [7, 17]. Yet, a common practice is to collect data from varying sensor locations, using both fixed and moving sensors. The aim is to mimic the availability of a (much) larger set of sensors or of a (much) higher number of data acquisition channels in the sensor digitization system. Several successive data sets are recorded, with sensors at different locations on the structure. Some of the sensors, called the reference sensors, are kept fixed, while the others are moved. Typically, it is based on 16–32 sensors, and can mimic a situation in which hundreds of channels are available. This set-up is referred to as *multi-patch measurements* set-up in this paper.

Processing multi-patch measurements data for structural analysis is often achieved by performing eigenstructure identification for each record separately, and then merging the results obtained for records corresponding to different sensor pools. However, pole matching may not be easy in practice, and thus the result of eigenvector gluing may not be consistent [18, 19]. Therefore, the question arises to perform eigenstructure identification by merging the data of the successive records, and processing them globally, instead of merging the identification results.

The purpose of this paper is to investigate how subspace-based covariance-driven output-only modal analysis algorithms can be adapted to handle a multi-patch measurements set-up, in the presence of an unmeasured and non-stationary excitation.

In section 2, the models are introduced and output-only covariance-driven subspace-based modal analysis methods are briefly reviewed. The mathematical modelling of the multi-patch measurements set-up is stated in section 3. A first merge of data is proposed for the case of a stationary excitation. This merge is shown to fail in the case of a non-stationary excitation. For the latter case, a covariance normalization prior to merge is introduced, and a simple implementation is given. Numerous experimental results obtained, on both laboratory and real application examples, are reported in section 4. Finally, some conclusions are drawn in section 5.

2. OUTPUT-ONLY SUBSPACE-BASED MODAL ANALYSIS

In this section, structural vibration analysis and subspace-based identification algorithms are briefly reviewed. First, the modelling issues are introduced, and then output-only covariance-driven subspace identification is recalled. The reader is referred to reference [20] for an overview of modal analysis methods.

2.1. MODELLING

The use of state-space representations for modal analysis is well known [3, 4, 13]. The main equations and parameters are briefly recalled, in order to introduce the notations. It is assumed that the behavior of the mechanical system can be described by a stationary linear dynamical system, and that, in the frequency range of interest, the input forces can be

modelled as a non-stationary white noise. This results in the following matrix differential equation:

$$M\ddot{\mathscr{Z}}(t) + C\dot{\mathscr{Z}}(t) + K\mathscr{Z}(t) = v(t), \qquad Y(t) = L\mathscr{Z}(t), \tag{1}$$

where t denotes continuous time; M, C, K are the mass, damping and stiffness matrices, respectively; (high dimensional) vector $\mathscr{Z}$ collects the displacements of the degrees of freedom of the structure; the external (non-measured) force v is modelled as a non-stationary white noise with time-varying covariance matrix $Q_v(t)$; measurements are collected in the (often, low dimensional) vector Y, and matrix L—made of 0's and 1's—indicates which components of the state vector are actually measured, namely where the sensors are located. The modes or eigenfrequencies denoted generically by μ, and the mode shapes or eigenvectors denoted generically by ψ_μ, are solutions of

$$\det(M\mu^2 + C\mu + K) = 0, \qquad (M\mu^2 + C\mu + K)\,\Psi_\mu = 0, \qquad \psi_\mu = L\Psi_\mu. \tag{2}$$

Sampling the model in equation (1) at rate $1/\tau$ yields the discrete time model in state-space form:

$$X_{k+1} = F\,X_k + V_{k+1}, \qquad Y_k = H\,X_k, \tag{3}$$

where the state and the output are

$$X_k = \begin{bmatrix} \mathscr{Z}(k\tau) \\ \dot{\mathscr{Z}}(k\tau) \end{bmatrix}, \qquad Y_k = Y(k\tau), \tag{4}$$

the state transition and observation matrices are

$$F = \mathrm{e}^{\mathscr{L}\tau}, \quad \mathscr{L} = \begin{bmatrix} 0 & I \\ -M^{-1}K & -M^{-1}C \end{bmatrix}$$

and

$$H = [L \quad 0]. \tag{5}$$

The measurement equation in equation (4) with H as in equation (5) implicitly assumes that the available sensors measure the (relative) displacements of the degrees of freedom themselves, namely are constraint gauges. If constraint gauges, velocity sensors and accelerometers are available, the measurement equation in equation (1) should be written as

$$Y(t) = \begin{pmatrix} L\mathscr{Z}(t) \\ N\dot{\mathscr{Z}}(t) \\ P\ddot{\mathscr{Z}}(t) \end{pmatrix}$$

with L, N, P made of 0's and 1's, and system (4) should be understood with

$$H = \begin{pmatrix} L & 0 \\ 0 & N \\ -PM^{-1}K & -PM^{-1}C \end{pmatrix}.$$

Consequently, state-space model (4) can always be enforced, whatever the sensors are. The nature of the sensors used only influences the observation matrix H.

In equation (4), the state noise V_{k+1} is *unmeasured*, Gaussian, zero-mean, white, with covariance matrix

$$Q_{k+1} \stackrel{\text{def}}{=} \mathbf{E}(V_{k+1}\ V_{k+1}^{\mathrm{T}}) = \int_{k\tau}^{(k+1)\tau} \mathrm{e}^{\mathscr{L}s}\ \tilde{Q}(s)\ e^{\mathscr{L}^{\mathrm{T}}s}\mathrm{d}s,$$

where $\mathbf{E}(\cdot)$ denotes the expectation operator and

$$\tilde{Q}(s) = \begin{bmatrix} 0 & 0 \\ 0 & M^{-1}Q_v(s)M^{-\mathrm{T}} \end{bmatrix}.$$

The whiteness assumption on the state noise and the absence of measurement noise in equation (3) are discussed in section 4.1. It is stressed that sinusoidal or colored noise excitation can be encompassed as well [5]. State X and observed output Y have dimensions $2m$ and r, respectively, with r (often much) smaller than $2m$ in practice. These issues are further discussed in section 4.

The modal parameters defined in equation (2) are equivalently found in the eigenstructure (λ, Φ_λ) of the state transition matrix F:

$$\mathrm{e}^{\tau\mu} = \lambda, \qquad \psi_\mu = \varphi_\lambda \stackrel{\text{def}}{=} H\ \Phi_\lambda.$$

The frequency and damping coefficient are recovered from a given eigenvalue λ through

$$\text{frequency} = \frac{a}{2\pi\tau}, \qquad \text{damping} = \frac{100\,|b|}{\sqrt{a^2+b^2}}, \qquad a = \left|\arctan\frac{\Im(\lambda)}{\Re(\lambda)}\right|, \qquad b = \ln|\lambda|.$$

Eigenvectors are real if $C = \alpha M + \beta K$, the simplest form of proportional damping. Because of the structure of the state in equation (4), the λ's and φ_λ's are pairwise complex conjugate. It is assumed that the system has no multiple eigenvalues. In addition, 0 is *not* an eigenvalue of state transition matrix F. The collection of pairs $(\lambda, \varphi_\lambda)$ form a canonical parameterization† of the pole part of the system in equation (3), referred to as the system eigenstructure.

2.2. OUTPUT-ONLY COVARIANCE-DRIVEN SUBSPACE IDENTIFICATION

Processing output covariance matrices is of interest for very large data sets, especially under non-stationary excitation. The difference between the covariance-driven form of subspace algorithms which is described here and the usual data-driven form [11] is minor, at least for eigenstructure identification [13].

Covariance-driven subspace identification of the eigenstructure $(\lambda, \varphi_\lambda)$'s is based on the following steps. Let $R_i \stackrel{\text{def}}{=} \mathbf{E}\ Y_k\ Y_{k-i}^{\mathrm{T}}$ and

$$\mathscr{H}_{p+1,q} \stackrel{\text{def}}{=} \begin{pmatrix} R_0 & R_1 & \vdots & R_{q-1} \\ R_1 & R_2 & \vdots & R_q \\ \vdots & \vdots & \vdots & \vdots \\ R_p & R_{p+1} & \vdots & R_{p+q-1} \end{pmatrix} \stackrel{\text{def}}{=} \text{Hank}\,(R_i), \tag{6}$$

†A parameterization invariant w.r.t. changes in the state basis.

be the theoretical output-covariance and Hankel matrices respectively. Introducing the cross-covariance between the state and the observed outputs

$$G \stackrel{\text{def}}{=} \mathbf{E}\ X_k\ Y_k^{\mathrm{T}},$$

direct computations of the R_i's from the model equations lead to

$$R_i = H\ F^i\ G \tag{7}$$

and to the well-known [21] factorization

$$\mathscr{H}_{p+1,q} = \mathscr{O}_{p+1}(H, F)\ \mathscr{C}_q(F, G), \tag{8}$$

where

$$\mathscr{O}_p(H, F) \stackrel{\text{def}}{=} \begin{pmatrix} H \\ HF \\ \vdots \\ HF^{p-1} \end{pmatrix} \quad \text{and} \quad \mathscr{C}_q(F, G) \stackrel{\text{def}}{=} (G\ FG \cdots F^{q-1}G)$$

are the observability and controllability matrices respectively.

The observation matrix H is then found in the first block-row of the observability matrix $\mathscr{O}$. The state-transition matrix F is obtained from the shift invariance property of $\mathscr{O}$, namely,

$$\mathscr{O}_p^{\uparrow}(H, F) = \mathscr{O}_p(H, F)\ F, \quad \text{where } \mathscr{O}_p^{\uparrow}(H, F) \stackrel{\text{def}}{=} \begin{pmatrix} HF \\ HF^2 \\ \vdots \\ HF^p \end{pmatrix}.$$

Of course, for recovering F, it is needed to assume that $\operatorname{rank}(\mathscr{O}_p) = \dim F$, and thus that the number of block-rows in $\mathscr{H}_{p+1,q}$ is large enough. The eigenstructure (λ, Φ_λ) results from

$$\det(F - \lambda\ I) = 0,\ F\ \Phi_\lambda = \lambda\ \Phi_\lambda.$$

The actual implementation of this subspace algorithm, known under the name of balanced realization (BR) [22, 23] has the empirical covariances

$$\hat{R}_i = \frac{1}{N} \sum_{k=1}^{N} Y_k\ Y_{k-i}^{\mathrm{T}} \tag{9}$$

substituted for R_i in $\mathscr{H}_{p+1,q}$, yielding the empirical Hankel matrix $\hat{\mathscr{H}}_{p+1,q} \stackrel{\text{def}}{=} \operatorname{Hank}(\hat{R}_i)$. How to select the number of lags $(p + q)$ and thus the size of $\hat{\mathscr{H}}_{p+1,q}$ is discussed in section 4.1. The SVD of $\hat{\mathscr{H}}_{p+1,q}$ and its truncation at the desired model order yield, in the left factor, an estimate $\hat{\mathscr{O}}$ for the observability matrix $\mathscr{O}$:

$$\begin{aligned} \hat{\mathscr{H}} &= U\ \Delta\ V^{\mathrm{T}} \\ &= U \begin{pmatrix} \Delta_1 & 0 \\ 0 & \Delta_0 \end{pmatrix} V^{\mathrm{T}}, \\ \hat{\mathscr{O}} &= U\ \Delta_1^{1/2}, \qquad \hat{\mathscr{C}} = \Delta_1^{1/2}\ V^{\mathrm{T}}. \end{aligned}$$

From $\hat{\mathscr{O}}$, estimates $(\hat{H}, \hat{F})$ and $(\hat{\lambda}, \hat{\boldsymbol{\phi}}_\lambda)$ are recovered as sketched above.

The CVA algorithm basically applies the same procedure to a Hankel matrix pre- and post-multiplied by the covariance matrix of future and past data respectively [24, 26].

The key feature in this algorithm is the factorization in equation (7), resulting in the factorization in equation (8), where the left factor $\mathcal{O}$ only depends on the pair (H, F), and thus on the eigenstructure of the system in equation (3), whereas the excitation V_k only affects the right factor $\mathcal{C}$ through the cross-covariance matrix G. This feature is now elaborated upon for handling multi-patch measurements set-ups.

3. MULTI-PATCH SUBSPACE-BASED MODAL ANALYSIS

Instead of a single record for the output (Y_k) of the system in equation (3), J records are now available

$$\underbrace{\begin{pmatrix} Y_k^{(0,1)} \\ Y_k^{(1)} \end{pmatrix}}_{\text{Record 1}} \quad \underbrace{\begin{pmatrix} Y_k^{(0,2)} \\ Y_k^{(2)} \end{pmatrix}}_{\text{Record 2}} \cdots \underbrace{\begin{pmatrix} Y_k^{(0,J)} \\ Y_k^{(J)} \end{pmatrix}}_{\text{Record } J}, \tag{10}$$

collected successively. Each record j contains data $Y_k^{(0,j)}$ from a fixed *reference* sensor pool, and data $Y_k^{(j)}$ from a *moving* sensor pool. The number of sensors may be different in the fixed and the moving pools, and thus in each record j, the dimensions r_0 of $Y_k^{(0,j)}$ and r_j of $Y_k^{(j)}$ may be different. This is referred to as *multi-patch measurements set-up* in the sequel.

The rest of the section is organized as follows. First, the mathematical modelling of the multi-patch measurements set-up is stated. Then, a first merge of data is proposed for the stationary excitation case, and is shown to fail in the non-stationary one. For the latter case, a covariance normalization prior to merge is introduced, and its implementation is given.

3.1. MODELING THE MULTI-PATCH MEASUREMENTS SET-UP

To each record j $(1 \leqslant j \leqslant J)$ corresponds a state-space realization in the form

$$\begin{aligned} X_{k+1}^{(j)} &= F\, X_k^{(j)} + V_{k+1}^{(j)}, \\ Y_k^{(0,j)} &= H_0\, X_k^{(j)} \quad \text{(reference pool)}, \\ Y_k^{(j)} &= H_j\, X_k^{(j)} \quad \text{(sensor pool No } j\text{)} \end{aligned} \tag{11}$$

with a single state transition matrix F—since the same system is being observed, a fixed observation matrix H_0 for the fixed sensor pool, and a specific observation matrix H_j corresponding to location j of the moving sensor pool.

The problem in finding out how to adapt the output-only covariance-driven subspace algorithm of section 2 in order to identify the eigenstructure of F in equation (11), on the basis of measurements (10) which should be merged somehow for this purpose. At this point, two facts should be stressed. First, the cornerstone in section (2) is factorization (7) which, of course, holds for each of the J records with a *different* left factor H and a *different* right factor G. In particular, even though the empirical estimates of the covariances $\mathbf{E}\, Y_k^{(j)}\, Y_{k-i}^{(j)\mathrm{T}}$ of the moving sensor pool can be computed, they are of little help because their factorizations (7) show up a record-dependent state-output correlation G since the sensors' location change. Second, the cross-record covariances $\mathbf{E}\, Y_k^{(j')}\, Y_{k-i}^{(j)\mathrm{T}}$ with $j \neq j'$ cannot be estimated, since sensor pools j and j' do not record data simultaneously. Thus, it is not possible to stack all the data sets in a unique vector, otherwise incomplete covariance matrices would have to be handled.

A consequence of those two facts, in the perspective of building a Hankel matrix enjoying a factorization property, is to concentrate on the covariances involving the *reference sensors*. From now on, the focus is on the following two families of covariances:

$$R_i^{0,j} \stackrel{\text{def}}{=} \mathbf{E}\ Y_k^{(0,j)}\ Y_{k-i}^{(0,j)^{\mathrm{T}}}, \quad R_i^j \stackrel{\text{def}}{=} \mathbf{E}\ Y_k^{(j)}\ Y_{k-i}^{(0,j)^{\mathrm{T}}} \tag{12}$$

of which empirical estimates can be computed, for lags $i \geqslant 0$. For describing the proposed solution to multi-patch subspace identification, the stationary and non-stationary input excitation cases are distinguished. A first merge of the data is now proposed for the stationary input excitation case. For investigating the non-stationary case, a simplifying assumption is introduced first, enforcing stationary excitation within the records, and record-dependent covariance matrix. This data merging is shown to fail in that non-stationary case. In section 3.4, an alternative merge of the data is introduced, based on a covariance normalization prior to merge for the simplified case of record-dependent excitation, and its implementation is given. The truly non-stationary case, where the excitation is time varying within each record, is a more realistic, yet much more difficult, situation to cope with. The interested reader is referred to reference [27] for technical details of theorems proving that the proposed method still works in that case.

3.2. DATA MERGING IN THE STATIONARY CASE

In the stationary case, the excitation covariance matrix does not depend on record j: $\mathbf{E}\ V_k^{(j)} V_k^{(j)^{\mathrm{T}}} = Q\ \delta(k - k')$, and the cross-covariance between the state and the fixed sensors output

$$G \stackrel{\text{def}}{=} \mathbf{E}\ X_k^{(j)}\ Y_k^{(0,j)^{\mathrm{T}}},$$

does *not* depend on j either. Therefore, for all the records $j = 1, \ldots, J$ and lags $i \geqslant 0$, the covariances in equation (12) factor out, with a constant *right* factor, as

$$\begin{aligned} R_i^{0,j} &= H_0\ F^i\ G \stackrel{\text{def}}{=} R_i^0, \\ R_i^j &= H_j\ F^i\ G. \end{aligned} \tag{13}$$

Consequently, for each lag $i \geqslant 0$, the R_i^j's can be stacked into a block-column vector

$$R_i^\pi \stackrel{\text{def}}{=} \begin{pmatrix} R_i^0 \\ R_i^1 \\ \vdots \\ R_i^J \end{pmatrix}, \tag{14}$$

which factors out as

$$R_i^\pi = H\ F^i\ G, \tag{15}$$

where H is the block-column of observation matrices

$$H \stackrel{\text{def}}{=} \begin{pmatrix} H_0 \\ H_1 \\ \vdots \\ H_J \end{pmatrix}. \tag{16}$$

Therefore, the Hankel matrix filled with those column-stacked covariances[‡] factors out as

$$\mathscr{H}^{\pi} \stackrel{\text{def}}{=} \text{Hank}\,(R_i^{\pi}) = \mathscr{O}(H, F)\,\mathscr{C}(F, G) \tag{17}$$

and the algorithm described in section 2 for the standard case can be applied to $\mathscr{H}^{\pi}$. In other words, when the input excitation is stationary, it can be proceeded as if the full set of sensor data were available altogether, instead of sensor pools with varying locations. In this case, direct application of the subspace algorithm to the column-stacked covariances (14) is a simple solution to the multi-patch output-only eigenstructure identification problem.

3.3. WHY THIS MERGE FAILS UNDER NON-STATIONARY EXCITATION

If the input excitation covariance matrix is assumed to depend on the record index j:

$$\mathbf{E}\; V_k^{(j)}\; V_{k'}^{(j)\mathrm{T}} = Q_j\; \delta(k - k'), \tag{18}$$

the cross-covariance matrix

$$G_j \stackrel{\text{def}}{=} \mathbf{E}\; X_k^{(j)}\; Y_k^{(0,j)\mathrm{T}},$$

also *depends on* j. Hence, for $j = 1, \ldots, J$ *and* $i \geqslant 0$, factorizations (13) should now be written with a record-dependent G

$$R_i^{0,j} = H_0\; F^i\; G_j, \qquad R_i^j = H_j\; F^i\; G_j \tag{19, 20}$$

and vector R_i^{π} of stacked covariances defined in equation (14) no longer factors out as in equation (15). As a consequence, brute force application of subspace algorithm by stacking the R_i^j's is not an appropriate solution to the eigenstructure identification problem in the case of record-dependent input excitation noise. To circumvent this difficulty, the idea is to *normalize* the covariance matrices (19) and (20) to make them appear as if they were obtained with the same excitation.

3.4. NON-STATIONARY EXCITATION: DATA NORMALIZATION PRIOR TO MERGE

For finding the appropriate normalization of the covariances, different covariance stacking operations are performed for the data from the reference and moving sensors respectively. In what follows, the generic notations introduced in section 2 are used.

3.4.1. *Reference sensors*

Thanks to equation (19), all the Hankel matrices built on the data delivered by the reference sensors of the J records factor out with the same *left* factor as

$$\mathscr{H}_{0,j} \stackrel{\text{def}}{=} \text{Hank}(R_i^{(0,j)}) = \mathscr{O}(H_0, F)\,\mathscr{C}(F, G_j). \tag{21}$$

One can thus proceed as follows. Let $R_i^0 \stackrel{\text{def}}{=} (R_i^{0,1}\; R_i^{0,2}\; \ldots\; R_i^{0,J})$ be the block-row vector of the entire set of reference data covariances. It factors out as

$$R_i^0 = H_0\; F^i\; G, \quad \text{where } G \stackrel{\text{def}}{=} (G_1\; G_2 \ldots G_J). \tag{22}$$

[‡] This Hankel matrix has $(J + 1)$ times as many rows as columns.

Thus, the Hankel matrix filled with those row-stacked covariances[§] also factors out as

$$\mathscr{H}_0 \stackrel{\text{def}}{=} \text{Hank}\,(R_i^0) = \mathscr{O}(H_0, F)\,\mathscr{C}(F, G). \tag{23}$$

Note that matrix $\mathscr{H}_0$ can be obtained by interleaving the block-columns of the J Hankel matrices $\mathscr{H}_{0,j}$ in equation (21). Assume that pair (H_0, F) is observable. Then, partitioning the right factor $\mathscr{C}$ of equation (23) in the same manner as G in equation (22), the right factors $\mathscr{C}(F, G_j)$ of equation (21) for all $j = 1, \ldots, J$ are recovered. Note that processing the reference data $Y_k^{(0,j)}$ *altogether*, on the basis of the *single* Hankel matrix factorization (23), is mandatory for making sure that the *same* state bases are dealt with in equation (11).

3.4.2. *Moving sensors*

Thanks to equation (20), the Hankel matrix built on the covariances of the data $Y_k^{(j)}$ from the moving sensor pool in record j enjoys a record-dependent factorization

$$\mathscr{H}_j \stackrel{\text{def}}{=} \text{Hank}(R_i^j) = \mathscr{O}(H_j, F)\,\mathscr{C}(F, G_j). \tag{24}$$

Assume that, for all j, the pair (F, G_j) is controllable. This is a reasonable assumption, since it just states that, while the excitation may change, it is required to excite all the modes of the system, for each record. Assume also that, up to a permutation on the record indexes, $C(F, G_1)$ is the best conditioned controllability matrix among the $\mathscr{C}(F, G_j)$s. In other words, assume that the best excitation of the system modes is achieved in record 1. The idea is then to assign that excitation to all the records through a normalization of the output covariances which is described now.

For all j, $j = 1, \ldots, J$, the following normalized matrices are defined:

$$\bar{\mathscr{H}}_j \stackrel{\text{def}}{=} \mathscr{H}_j\,(\mathscr{C}^{\text{T}}(F, G_j)(\mathscr{C}(F, G_j)\,\mathscr{C}^{T}(F, G_j))^{-1}\,\mathscr{C}(F, G_1)) \tag{25}$$

$$= \mathscr{O}(H_j, F)\,\mathscr{C}(F, G_1). \tag{26}$$

It should be noted that $\bar{\mathscr{H}}_j$ coincides with the Hankel matrix Hank $(\bar{R}_i^j)$ built on covariances $\bar{R}_i^j$ which factor out as

$$\bar{R}_i^j = H_j\,F^i\,G_1. \tag{27}$$

Therefore, one can now proceed as in the case of constant excitation covariance matrix. For each lag $i \geqslant 0$, the following block-column stacked covariances are defined:

$$\bar{R}_i \stackrel{\text{def}}{=} \begin{pmatrix} \bar{R}_i^0 \\ \bar{R}_i^1 \\ \vdots \\ \bar{R}_i^J \end{pmatrix}, \quad \text{where } \bar{R}_i^0 \stackrel{\text{def}}{=} R_i^{0,1} = H_0\,F^i\,G_1. \tag{28}$$

Thanks to equation (27), those stacked covariances $\bar{R}_i$ behave as R_i^{π} defined in equation (14): they factor out as $\bar{R}_i = H\,F^iG_1$, with H defined in equation (16). Therefore, the Hankel matrix filled with those column-stacked covariances[¶] factors out as

$$\bar{\mathscr{H}} \stackrel{\text{def}}{=} \text{Hank}(\bar{R}_i) = \mathscr{O}(H, F)\,\mathscr{C}(F, G_1). \tag{29}$$

Thanks to equation (29), the algorithm given in section 2 can be applied to $\bar{\mathscr{H}}$.

[§] This Hankel matrix has J times as many columns as rows.
[¶] This Hankel matrix has $(J + 1)$ times as many rows as columns.

Note that matrix $\bar{\mathscr{H}}$ can be obtained by interleaving the block-rows of $\bar{\mathscr{H}}_0 \stackrel{\text{def}}{=} \text{Hank}(\bar{R}_1^0) = \mathscr{H}_{0,1}$ and of the J matrices $\bar{\mathscr{H}}_j$ defined in equation (25). Note also that the computation of all the normalized covariance matrices in equation (27) is not necessary. How to implement the above reasoning is made clear now.

3.4.3. *Algorithm*

The following algorithm is proposed, where J is the number of records and $\hat{M}$ denotes an empirical estimate of matrix M.

- Build the J Hankel matrices $\hat{\mathscr{H}}_{0,j} = \text{Hank}(\hat{R}_i^{(0,j)})$ from the reference sensor data.
- Build $\hat{\mathscr{H}}_0$ by interleaving the block-columns of the J matrices $\hat{\mathscr{H}}_{0,j}$'s ($j = 1, \ldots, J$).
- SVD-decompose $\hat{\mathscr{H}}_0$. Keep only the right factor $\mathscr{C}(F, G)$ in equation (23), and call it just $\mathscr{C}$.
- Partition $\mathscr{C}$ into $\mathscr{C} \stackrel{\text{def}}{=} (\mathscr{C}_1\ \mathscr{C}_2 \ldots \mathscr{C}_J)$ as G in equation (22). Assume $\mathscr{C}_1$ is the best conditioned of the $\mathscr{C}_j$'s.
- Compute the normalizing factors $(\mathscr{C}_j^{\mathrm{T}}\ (\mathscr{C}_j \mathscr{C}_j^{\mathrm{T}})^{-1}\ \mathscr{C}_1)$.
- Build the J Hankel matrices $\hat{\mathscr{H}}_j = \text{Hank}(\hat{R}_i^j)$ from the moving sensor data.
- Compute the J normalized matrices $\bar{\mathscr{H}}_j \stackrel{\text{def}}{=} \hat{\mathscr{H}}_j\ (\mathscr{C}_j^{\mathrm{T}}\ (\mathscr{C}_j \mathscr{C}_j^{\mathrm{T}})^{-1}\ \mathscr{C}_1)$. Define $\bar{\mathscr{H}}_0 \stackrel{\text{def}}{=} \hat{\mathscr{H}}_{0,1}$.
- Build $\bar{\bar{\mathscr{H}}}$ by interleaving the block-rows of the $(J+1)$ matrices $\bar{\mathscr{H}}_j$'s ($j = 0, \ldots, J$).
- Apply the algorithm of section 2 to $\bar{\bar{\mathscr{H}}}$.

The following comments are in order. First, the computational complexity of this algorithm does *not* depend on the number J of records, since the smallest dimension of the two Hankel matrices $\hat{\mathscr{H}}_0$ and $\bar{\bar{\mathscr{H}}}$ to be decomposed depends only on the number of reference sensors. Second, the interleaving of the block-rows of the $\bar{\mathscr{H}}_j$'s can be done even when the number of sensors in the moving pools is *not* constant: the measurement vectors $Y_k^{(j)}$ and $Y_k^{(j')}$ may have different dimensions. Third, it is not needed to compute explicitly the G_j matrices, since only the right factors $\mathscr{C}(F, G_j)$ in equation (24) are needed for computing $\bar{\mathscr{H}}_j$ in equation (25).

4. APPLICATION EXAMPLES

In this section, numerical results are reported, which have been obtained for two application examples of the multi-patch subspace identification approach to structural vibration analysis proposed in section 3.4. The first one is a real outdoor bridge, with the help of which it is investigated how to handle records with different number of moving sensors. The second one is a laboratory testbed, with the help of which it is investigated as to how sensors data in different directions and/or with different excitation directions can be merged.

Before proceeding, some comments are in order on the practical use of the classical (monoreference and full covariance) subspace identification algorithm of section 2.

4.1. PRACTICAL ISSUES IN SUBSPACE EIGENSTRUCTURE IDENTIFICATION

The selection of the model order, and thus of the size of the Hankel matrices on the one hand, and the handling of the presence and nature of excitation and measurement noises on the other, are two major practical issues which are addressed now.

As stressed in references [5, 15, 13], when few sensors are available, a number of modes which is much smaller than the number of solutions of equation (2), but much larger than

the number of sensors, can be identified. In order to extract the modes from the data, the subspace method must be applied with an increasing SVD truncation order and the relevant modes must be searched for in the frequency band of interest. Since the subspace method yields a set of modes with both structural—from the structure *and* the excitation—and spurious mathematical modes, a practical method to distinguish between the two types of modes is needed. Fortunately, spurious modes tend to vary from one model order to the next; which is why usage suggests to plot the frequencies against SVD truncation order, in a stability or stabilization diagram [8, 13, 25, 18]. This procedure is used in the sequel to display our results.

Numerous experiments with the classical subspace method have shown that:

- It is of no practical help to select for $\mathscr{H}_{p+1,q}$ in equation (6) values other than $q = p + 1$. The number of lags $2p$ for the data covariances should be large (typically more than two hundreds in the experiments below).
- The number of modes should be overestimated, because modes tend to stabilize, and even to show up, for high orders. In other words, the SVD in the algorithm of section 2 should be truncated at an order much greater than the "theoretical" order, that is $2m/r - 1$, where m is the number of desired modes and r is the number of sensors.

An excitation noise at a single constant frequency is recognized as a pole by the algorithm of section 2, designed under the assumption of a white excitation noise. Such a pole can be eliminated provided that prior information is available. This is the case of the harmonics of the rotation speed for rotating machines with load unbalancing. Similarly, a colored excitation noise can be easily eliminated provided that its poles are (significantly) more damped than those of the structure. It is also a common finding that the poles of the structure tend to stabilize when the Hankel matrix order is increased, whereas those of the excitation mostly do not. A non-stationary excitation is actually a favorable situation, since the averaging performed in equation (9) for computing G tends to whiten the noise. This is the case of a chirp-like non-stationary excitation.

Because of the above, the multi-patch identification method has been implemented as follows. Since the Hankel matrix $\bar{\mathscr{H}}$ is built on stacked covariances (28), its SVD truncation order should be taken to be no greater than $q \times r_0/r$, where $r = r_0 + \sum_{j=1}^{J} r_j$, and where r_0 is the number of reference sensors and r_j the number of sensors in record j of equation (10).

If a measurement noise is enforced in equation (3), then the Hankel matrix in equation (6) should be filled with delayed covariances [26].

4.2. REAL EXAMPLE

Multi-patch identification results obtained on the first application example, a real bridge [30], are now shown.

4.2.1. *The Z24 bridge and its modes*

The proposed method has been applied to the Swiss Z24 bridge, a benchmark of the BRITE/EURAM project SIMCES on identification and monitoring of civil engineering structures, for which EMPA[‖] has carried out tests and data recording. The response of the

[‖] EMPA is the Swiss Federal Laboratories for Materials Testing and Research.

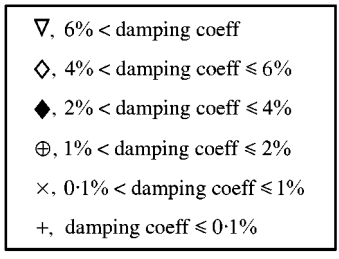

Figure 1. Meaning of the symbols used in Figures 2–4, and Figures 8–11.

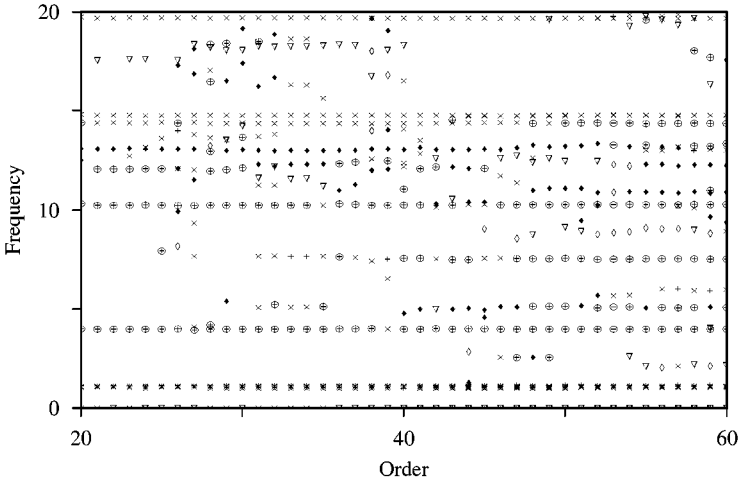

Figure 2. Z24 bridge—classical subspace identification: first record (three sensors).

bridge to traffic excitation under the bridge has been measured in 135 points, mainly in the vertical and transverse directions, and sampled at 100 Hz. Because at most 19 sensors were available, nine data sets have been recorded, each containing the measurements from four fixed and 15 moving sensors. However, it is not recommended to merge data recorded under very different temperature and traffic conditions [31], and to mix different directions [5]. Therefore, for investigating the experimental properties of the proposed multi-patch subspace algorithm, $J = 2$ records have been selected from sensors in the vertical direction, with one reference sensor, and two moving sensors in the first record, and only one moving sensor in the second record. Each signal contains 65 535 samples. As mentioned above, processing more records would have affected the required memory size, but *not* the computational complexity. Also, it is of interest to investigate the practical relevance of the conceptual capability of the proposed algorithm to handle records with different numbers of moving sensors.

The classical subspace algorithm of section 2, based on full data covariances and on $q = 128$, has been applied separately to each record, which contain 3 and 2 sensors respectively. The results are displayed in Figures 2 and 3, where frequencies (ordinate) are displayed for increasing SVD truncation orders (abscissa), in a stabilization diagram whose symbols are given in Figure 1.

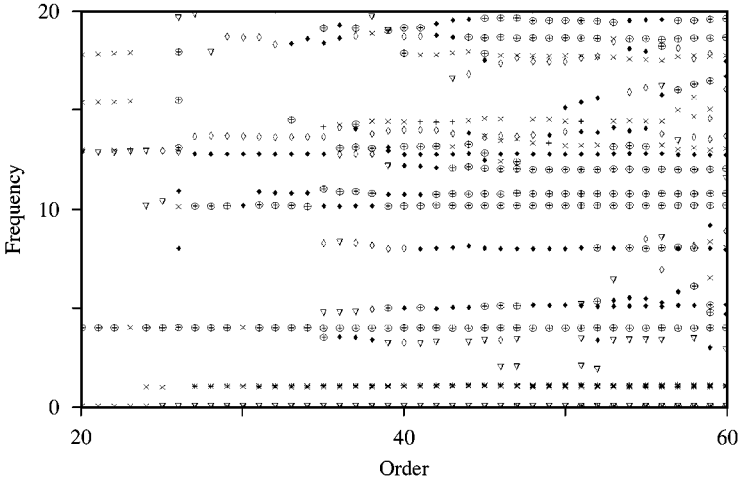

Figure 3. Z24 bridge—classical subspace identification: second record (two sensors).

TABLE 1

Estimated modes for the Z24 bridge (classical subspace identification)

Mode	1	2	3	4	5
Freq. (Hz)	4·0	5·3	9·8	10·3	12·0

Typical values of estimated modes which can be extracted from these diagrams are displayed in Table 1.

4.2.2. *Multi-patch identification*

The multi-patch subspace identification algorithm of section 3.4, based on partial covariances (12) and on $q = 128$, has been applied to the data from the two records. The results are displayed in Figure 4. Here, the SVD truncation order should be taken to be no greater than $128 \times 1/(1 + 2 + 1) = 32$. Figure 4 shows up several improvements over Figures 2 and 3, on several aspects. Actually, for large enough truncation order:

- Spurious modes disappear: around 1 Hz, for example;
- True modes appear and stabilize faster and fluctuate less in the diagrams: around 5.3 and 9.8 Hz, for example;
- The damping of the true modes is more accurately estimated, at lower orders than before, allowing to separate true and wrong modes among the stabilized ones: a wrong mode appears at 7 Hz with a high damping, whereas the true mode at 4 Hz appears with a low damping;
- Some modes, not identified in Figures 2 and 3, now show up in a stable diagram: around 12 Hz, among others.

Figure 4. Z24 bridge—multi-patch subspace identification: merging the two records.

The multi-patch method extracts seven modes in the range 0–11 Hz. Five of these modes come from the structure and tend to appear in many diagrams during the whole year. The 5.3 Hz mode is very difficult to extract, due mainly to low excitation at this frequency. In both classical identifications (Figures 2 and 3), it appears very late in the diagrams and has little stability, whereas those two points are improved in the multi-patch trial. Figure 4 is a remarkably clear diagram which, above a truncation order of 15, is cleaned from all spurious poles, even those which tend to stabilize in Figures 2 and 3. This appears to be an improvement w.r.t. the results in reference [18], where the stabilization diagrams resulting from merging different modal analyses are superimposed (but not smoothed) diagrams.

4.3. LABORATORY EXAMPLE

Multi-patch identification results obtained on the second application example, a laboratory set-up, are now shown.

4.3.1. *The steel-quake structure and its modes*

The steel-quake structure is used at the Joint Research Centre in Ispra (Italy) to test the performance of steel buildings during earthquakes. Experimental data from this structure have been proposed as a benchmark in the framework of the European COST F3 Structural Dynamics. The structure, shown in Figure 5, is a two-story frame. The structure is excited with the aid of an impact hammer. The resulting excitation is thus far from being a white noise. For each impact location, eight to 10 experiments are performed, resulting in different excitations. Different impact locations have been used, resulting in another cause of non-stationarity. The locations selected for the four impact tests are shown in Figure 6. Fifteen accelerometers are used for recording the reaction of the structure to the hammer impacts. The sampling frequency is 128 Hz, and for each channel 3200 data points are recorded. All these experiments yield data samples from the structure under different non-stationary excitations.

The sensor locations are shown in Figure 7, and the directions in which the measurements are taken are summarized in Table 2. Since the sensors' locations are the same for the four

Figure 5. The steel-quake structure.

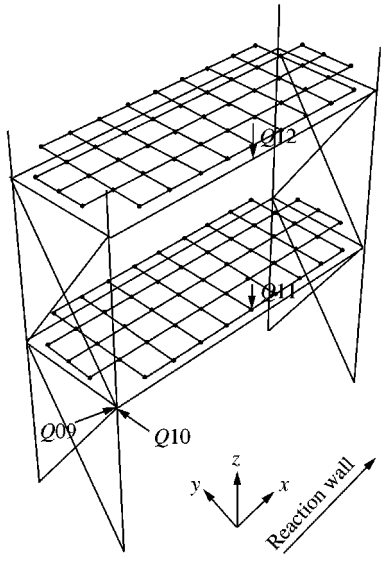

Figure 6. Steel-quake structure—excitation impact locations: $Q09$–$Q12$.

impact tests, multi-patch records as in equation (10) can be generated by selecting and grouping subsets of sensors from the different experiments. This results in non-stationary multi-patch records corresponding to model (11) and (18).

The classical subspace algorithm of section 2, based on full data covariances and on $q = 256$, has been applied to one set of 12 sensors data (all sensors except 3, 7, 10) from experiment $Q09$-1. The results are displayed in Figure 8. Typical values and directions of the estimated modes which can be extracted are displayed in Table 3. This is in agreement with the results in reference [28].

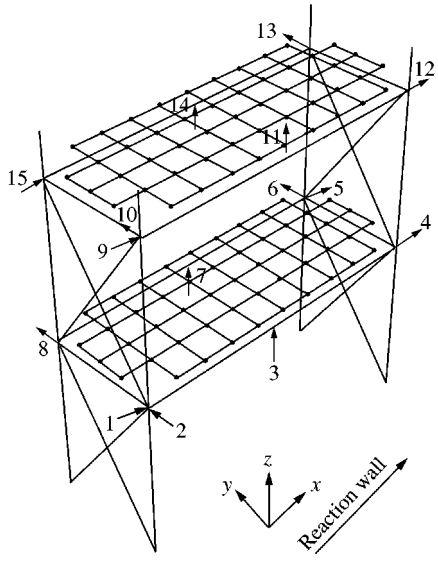

Figure 7. Steel-quake structure—sensors locations, with directions summarized in Table 2.

TABLE 2

Sensor directions, as displayed in Figure 7, for the steel-quake structure

Sensor No.	Direction	Sensor No.	Direction	Sensor No.	Direction
1	*X*	6	*Y*	11	*Z*
2	*Y*	7	*Z*	12	*X*
3	*Z*	8	*Y*	13	*Y*
4	*X*	9	*X*	14	*Z*
5	*X*	10	*Y*	15	*X*

4.3.2. *Multi-patch identification*

The multi-patch algorithm of section 3.4 has been applied to different configurations, corresponding to different sensor locations, different hammer excitations, different excitation locations. In each of the Figures 9–11, each record comes from a different excitation experiment. For example, in Figure 9, the references used are sensors 6 and 8, and the moving sensors are: sensors 11 and 14 from the first experiment of hammer location *Q*09, sensors 9 and 15 from the second experiment of hammer location *Q*10, sensors 1 and 4 from the third experiment of hammer location Q10, sensors 2 and 13 from the fourth experiment of hammer location *Q*09, and sensors 5 and 12 from the fifth experiment of hammer location *Q*10.

As mentioned in section 3.4, the computational cost of the method increases with the number of reference and moving sensors. However, the use of the low computational form of the SVD—which saves both memory space and computation time—makes it feasible to mix five records, each with four to five sensors. In this way, almost all the sensors data available for the steel-quake benchmark have been used.

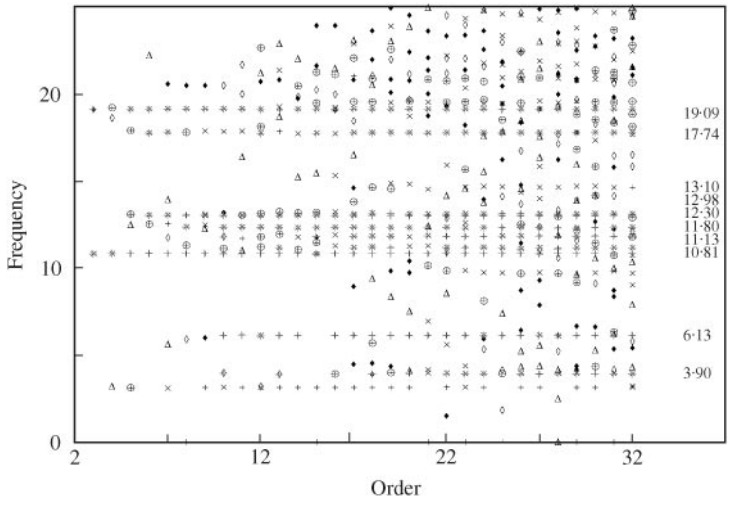

Figure 8. Steel-quake structure—classical subspace identification—12 sensors (all except sensors 3, 7, 10) (Q09–1).

TABLE 3

Some modes extracted from Figure 8, *for the steel-quake structure* (*classical subspace identification*)

Mode	Frequency (Hz)	Direction	Mode	Frequency (Hz)	Direction
1	3·1	X	5	10·8	X
2	3·92	Y	6	12·27	Z
3	6·1	Y	7	13·0	Z
4	9·68	Y	8	17·7	Z

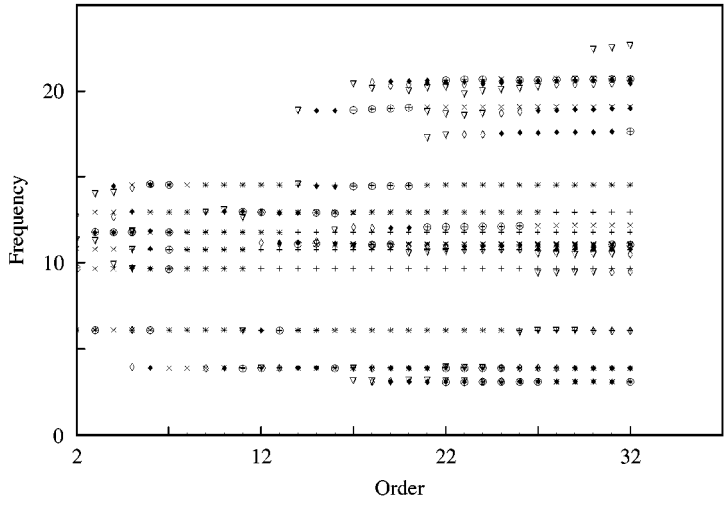

Figure 9. Steel-quake structure—multi-patch subspace identification—reference sensors: 6/8; moving sensors: 11/14 (Q09-1), 9/15 (Q10-2), 1/4 (Q10-3), 2/13 (Q09-4), 5/12 (Q10-5).

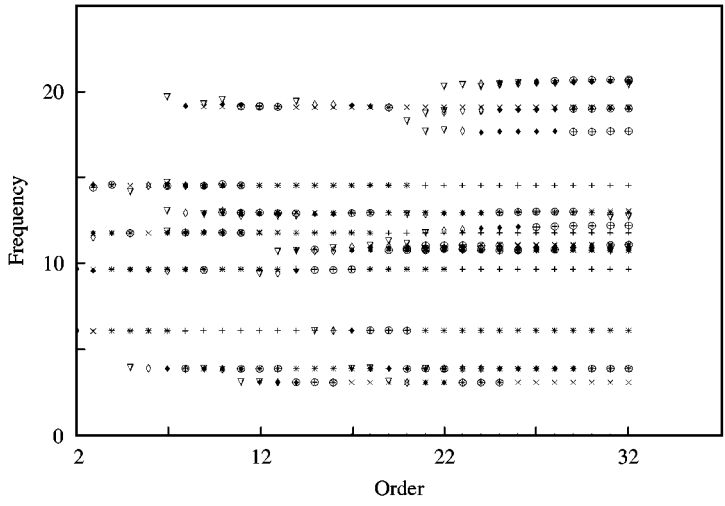

Figure 10. Steel-quake structure—multi-patch subspace identification—reference sensors: 1/6/7; moving sensors: 4/5 (Q09-1), 8/13 (Q10-2), 12/15 (Q10-3), 11/14 (Q09-4), 2/10 (Q09-5).

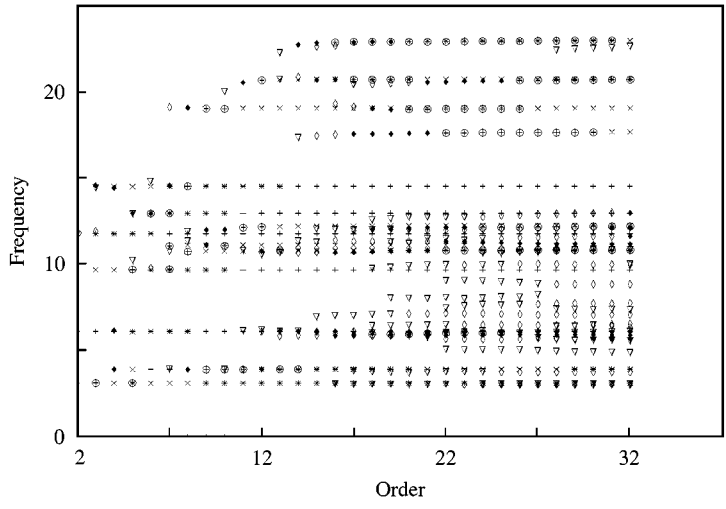

Figure 11. Steel-quake structure—multi-patch subspace identification—reference sensors: 4/5/12; moving sensors: 1/9/15 (Q10-1), 2/6/8/10/13 (Q10-2), 3/7/11/14 (Q10-3).

The multi-patch subspace identification algorithm, based on partial covariances (12) and on $q = 256$, has been applied to data from sessions Q09 to Q12, namely data merging the four excitations locations. However, since the results of all our experiments have not shown any qualitative difference between the use of the four sessions and only the first two ones, in the results shown below, the data which are used correspond to the excitation sessions Q09 and Q10 only.

Figure 9 displays the stabilization diagram of a multi-patch trial made with the sensors used for the results shown in Figure 8. The two excitation cases are merged: data from experiments Q09 and Q10 are used. Even though the multi-patch analysis handles

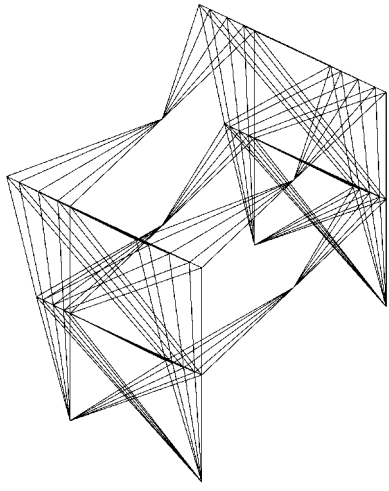

Figure 12. Steel-quake structure–multi-patch subspace identification—bending mode in Y direction at frequency 3·92 Hz, extracted from Figure 11.

covariance matrices of much smaller size (2×12) than the classical analysis (12×12), and is thus processing much less information, the stabilization diagram in Figure 9 is obviously cleaned out from spurious modes which appear in the stabilization diagram of the classical algorithm in Figure 8.

The stabilization diagram of a second multi-patch trial merging experiments $Q09$ and $Q10$ is displayed in Figure 10. Note that the diagram is good, even though the three reference sensors are in the three directions X, Y, and Z.

Now a result is shown which suggests how critical the grouping of the sensors in the pools of equation (11) is in influencing the extracted modeshapes. The stabilization diagram of a multi-patch trial with all the sensors is displayed in Figure 11. Note that the sensors are grouped according to the direction in which they measure. Since all the available sensors are used, the animated modeshapes[††] can be plotted: this is done in Figures 12–14 for three different frequencies. For each frequency, the selected modeshape has the highest MAC value. Taking the results in reference [28] as the reference modes and modeshapes, the modes and modeshapes in Figures 11–14 are well identified.

Comparison of Figure 11 with Figures 9 and 10 suggests that merging data from the two excitation sessions $Q09$ and $Q10$ leads to better diagrams than processing data from excitation $Q10$ only.

It should be pointed out that, theoretically, the eigenstructure identified by the multi-patch method does not depend on the choice of the reference and moving sensors, but only on the whole set of sensors available. However, due to numerical precision, the multi-patch method could be less stable than the classical subspace method. This can be observed sometimes in stabilization diagrams, which may not be the same for different choices of reference and moving sensors. But this effect may be more crucial for the modeshape extraction.

From numerous experiments, it turns out that a small number of sensors may be sufficient for finding many modes, provided that the sensors are well located, and in particular measure in the same direction. However, although only few sensors are needed to

[††] In no measurement point, all the d.o.f.'s are measured; hence the animation lacks.

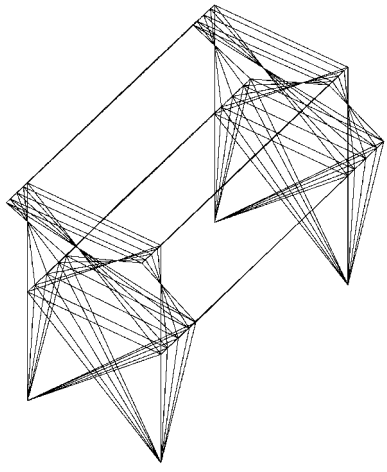

Figure 13. Steel-quake structure—multi-patch subspace identification—bending mode in X direction at frequency 10·8 Hz, extracted from Figure 11.

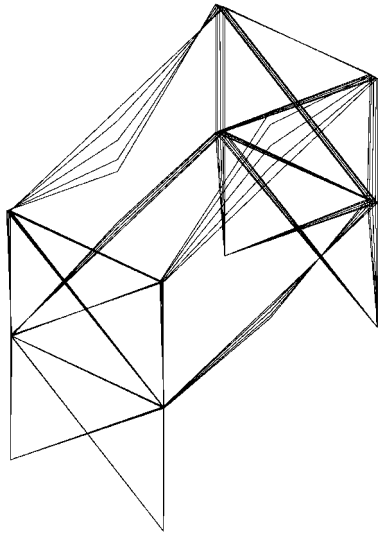

Figure 14. Steel-quake structure—multi-patch subspace identification—slab torsion in Z direction at frequency 17·7 Hz, extracted from Figure 11.

extract frequencies and damping coefficients, processing more sensors is of interest to obtain modeshapes with a larger number of components.

5. CONCLUSION

The multi-patch measurements set-up for output-only in-operation structural analysis has been discussed. In this type of set-up, several moving sensors mimic the availability of a much larger set of sensors. The proposed identification method consists in merging the

data first and processing them globally using an output-only covariance-based subspace algorithm. This has to be contrasted with classical multi-patch identification, which is usually performed by merging identification results obtained on the different records. The presence of an unmeasured and non-stationary excitation makes the issue of output data merging non-trivial. The key idea of the proposed method is a suitable normalization of the output covariances. This method, as well as the classical subspace identification algorithm [23], has been proved to provide us with consistent estimates of the eigenstructure, even under non-stationary excitation [27]. Numerical results of one laboratory set-up (steel-quake structure) and one real example ($Z24$ bridge) have been reported, which clearly highlight the potential benefits of the proposed method.

First, the method efficiently merges data by smoothing out the diagrams, rejecting spurious and instable frequencies. Actually, the averaging operation underlying the covariance computation, in combination with the key factorization property of the covariances, allows to cancel out non-stationarities in the excitation. Moreover, it appears that the introduction of different excitation conditions compensates somehow the loss of information due to the reduced size of the covariance matrices handled by the multi-patch algorithm.

Second, even with short record lengths, the natural frequencies are well estimated, whereas the modeshapes are more sensitive to the record length; this is in agreement with the results obtained for a bridge reported in reference [29].

Third, application of the multi-patch method over time is expected to further smooth out the effect of non-stationary excitation. Finally, the actual stability of the multi-patch diagrams makes the proposed multi-patch method a good candidate for a future automated identification procedure.

What the proposed algorithm is not capable of is to separate modes of the structure from the modes corresponding to the non–white excitation, but the classical subspace identification procedure is unable to achieve that either. Nevertheless, the new algorithm appears to perform well at extracting modes which appear only in some diagrams, for example modes which are not very well excited all the time. This feature is important in practice, and should hopefully be confirmed in further numerical investigations.

ACKNOWLEDGMENTS

The authors are indebted to the editor and the referees, whose careful reading and detailed comments helped in improving an earlier version of the paper.

Part of this work has been carried out within the framework of Eureka project 1562 SINOPSYS (model-based Structural monitoring using *IN-OP*eration *SYS*tem identification), co-ordinated by LMS, Leuven, Belgium.

REFERENCES

1. L. Hermans and H. Van der Auweraer 1999 *Mechanical Systems and Signal Processing* **13**, 193–216. Modal testing and analysis of structures under operational conditions: industrial applications.
2. E. Parloo, P. Verboven, P. Guillaume and M. Van Overmeire 2001 *Proceedings of the International Modal Analysis Conference*, 425– 431. Maximum likelihood identification of modal parameters from nonstationary operational data.
3. D. J. Ewins 1984 *Modal Testing*: *Theory and Practice*. Letchworth, Hertfordshire, U.K.: Research Studies Press.
4. J. N. Juang 1994 *Applied System Identification*. Englewood Cliffs, NJ: Prentice-Hall.

5. M. Prevosto, M. Olagnon, A. Benveniste, M. Basseville and G. Le Vey 1991 *Journal of Sound and Vibration* **148**, 329–342. State-space formulation, a solution to modal parameter estimation.
6. F. Lembregts, R. Snoeys and J. Leuridan 1987 *Journal of Modal Analysis* **2**, 19–31. Application and evaluation of multiple input modal parameter estimation.
7. F. Deblauwe, R. J. Allemang and D. L. Brown 1987 *Proceedings of the International Modal Analysis Conference*, 832–845. The polyreference time domain technique.
8. R. J. Allemang and D. L. Brown 1998 *Journal of Sound and Vibration* **211**, 301–322. A unified matrix polynomial approach to modal identification.
9. Q. J. Yang, P. Q. Zhang, C. Q. Li and X. P. Wu 1994 *Mechanical Systems and Signal Processing* **8**, 159–174. A system theory approach to multi-input multi-output modal parameters identification methods.
10. B. Ottersten, M. Viberg and T. Kailath 1992 *IEEE Transactions on Signal Processing* **40**, 590–599. Analysis of subspace fitting and ML techniques for parameter estimation.
11. P. Van Overschee and B. De Moor 1996 *Subspace Identification for Linear Systems*: *Theory*, *Implementation*, *Applications*. Dordrecht: Kluwer.
12. M. Viberg and B. Ottersten 1991 *IEEE Transactions on Signal Processing* **39**, 1110–1121. Sensor array processing based on subspace fitting.
13. B. Peeters and G. De Roeck 1999 *Mechanical Systems and Signal Processing* **13**, 855–878. Reference-based stochastic subspace identification for output-only modal analysis.
14. G. de Roeck, B. Peeters and W.-X. Ren 2000 *Proceedings of the International Modal Analysis Conference*, 1106–1112. Benchmark study on system identification through ambient vibration measurements.
15. M. Basseville, A. Benveniste, B. Gach-Devauchelle, M. Goursat, D. Bonnecase, P. Dorey, M. Prevosto and M. Olagnon 1993 *Mechanical Systems and Signal Processing* **7**, 401–423. Damage monitoring in vibration mechanics: issues in diagnostics and predictive maintenance.
16. M. Abdelghani, M. Goursat, T. Biolchini, L. Hermans and H. Van der Auweraer 1999 *Proceedings of the International Modal Analysis Conference*, 224–230. Performance of output-only identification algorithms for modal analysis of aircraft structures.
17. H. Vold, J. Kundrat, T. Rocklin and R. Russel 1982 *SAE Paper* 820194, *Transactions of SAE* **91**, 815-821. A multi-input modal parameter estimation algorithm for mini-computers.
18. H. Van der Auweraer, W. Leurs, P. Mas and L. Hermans 2000 *Proceedings of the International Modal Analysis Conference*, 763–771. Modal parameter estimation from inconsistent data sets.
19. R. L. Mayes and S. E. Klenke 2001 *Proceedings of the International Modal Analysis Conference*, 1023–1028. Consolidation of modal parameters from several extraction sets.
20. N. Maia and J. Silva 1997 *Theoretical and Experimental Modal Analysis*, Taunton U.K.: Research Studies Press.
21. P. Stoïca and R. L. Moses 1997 *Introduction to Spectral Analysis*. Englewood Cliffs, NJ: Prentice-Hall.
22. H. Akaïke 1974 *IEEE Transactions on Automatic Control* **19**, 667–674. Stochastic theory of minimal realization.
23. A. Benveniste and J-J. Fuchs 1985 *IEEE Transactions on Automatic Control* **30**, 66–74. Single sample modal identification of a non-stationary stochastic process.
24. H. Akaïke 1973 *SIAM Journal on Control* **13**, 162–173. Markovian representation of stochastic processes by canonical variables.
25. J. Cooper 1999 *Proceedings of the 2nd International Conference on Identification in Engineering Systems*, Swansea, U.K., 375–381. On the use of stability plots for modal parameter identification.
26. M. Basseville, M. Abdelghani and A. Benveniste 2000 *Automatica* **36**, 101–109. Subspace–based fault detection algorithms for vibration monitoring.
27. L. Mevel, A. Benveniste, M. Basseville and M. Goursat 2002 *IEEE Transactions on Signal Processing* 50. Blind subspace-based eigenstructure identification under nonstationary excitation using moving sensors.
28. J. B. Bodeux and J. C. Golinval 2000 *Proceedings of the European COST F3 Conference on System Identification and Structural Health Monitoring*, 303–312. ARMAV model technique for system identification and damage detection.

29. C. GENTILE and A. SAISI 2000 *Proceedings of the International Modal Analysis Conference*, 1320–1326. Accuracy assessment of bridge modal parameters estimated from ambient vibration measurements.
30. L. MEVEL, A. BENVENISTE, M. BASSEVILLE and M. GOURSAT 2001 *Proceedings of the International Modal Analysis Conference*. Polyreference subspace based modal identification of a concrete three span bridge.
31. B. PEETERS and G. DE ROECK 2000 *Proceedings of the International Modal Analysis Conference*, 1570–1576. One year monitoring of the Z24-bridge: environmental effects versus damage events.